3 Biotech (2026) 16:9
https://doi.org/10.1007/s13205-025-04611-z

ORIGINAL ARTICLE

Molecular dynamics simulation and structural characterization of (-)-carvone and cis-dihydrocarvone from *Mentha piperita* L. as potential MMP9 inhibitors for idiopathic pulmonary fibrosis therapy

G. Koteswara Reddy[1] · Yuvaraj Dinakarkumar[2] · Korukonda Satwik[1] · Allam Sai Sree Thanay[1] · Bobba Devi Sri Siddhartha[1] · Nandigum Sai Anvesh[1] · Selvaraj Arokiyaraj[3] · Panneerselvam Theivendren[4]

Received: 26 July 2025 / Accepted: 24 October 2025

Abstract

Idiopathic pulmonary fibrosis (IPF) is a progressive lung disease involving dysregulated matrix metalloproteinase-9 (MMP9) activity, leading to excessive extracellular matrix deposition and lung tissue deterioration. This study investigated bioactive compounds from *Mentha piperita* L. as potential MMP9 inhibitors for IPF therapy. Gas chromatography-mass spectrometry (GC–MS) analysis identified nine phytochemicals in the methanolic extract of peppermint leaves. Drug-likeness screening using Lipinski's Rule of Five identified two lead compounds: (-)-carvone and cis-dihydrocarvone. ADMET analysis revealed favorable pharmacokinetic properties, including appropriate solubility (−3.089 and −3.12, respectively) and blood–brain barrier permeability values (0.345 and 0.357). TOPKAT toxicity prediction classified both compounds as non-carcinogenic with negligible skin sensitization potential. Molecular docking against MMP9 (PDB ID: 1GKD) yielded MolDock scores of −84.22 for (-)-carvone and −87.47 for cis-dihydrocarvone, indicating strong binding affinity. Molecular dynamics simulations over 100 ns demonstrated stable protein–ligand complexes with consistent RMSD values (~0.8 Å for ligand), sustained hydrogen bonding interactions, and minimal conformational changes. Key residues LEU188, VAL398, HIS401, and TYR423 were identified as critical for binding stability. These computational findings establish (-)-carvone and cis-dihydrocarvone as promising MMP9 inhibitor candidates for IPF treatment, warranting in vitro and in vivo experimental validation.

Keywords Idiopathic pulmonary fibrosis (IPF) · Carvone · Cis-dihydrocarvone · Molecular dynamic simulations

Introduction

A significant proportion of the population presents with pathologies etiologically linked to unfavourable environmental stressors and other exogenous factors. Communicable diseases impair the immune system, contributing to non-communicable diseases (NCDs), which are significant threats worldwide (Kitole et al. 2024). Factors such as genetics, physiology, environment, and behaviour lead to NCDs, particularly affecting low- and middle-income countries, where they result in a majority of deaths (Liu et al. 2024). NCDs can be categorized into diabetes, cancer, chronic respiratory conditions, and cardiovascular illnesses, with common risk factors including poor diet, alcohol consumption, tobacco use, and lack of physical activity (Siiba et al. 2024). A multi-sectoral strategy focusing on prevention, early detection, and treatment is vital in combating

✉ Yuvaraj Dinakarkumar
yuvarajdinakarkumar@gmail.com

✉ Panneerselvam Theivendren
tpsphc@gmail.com

1 Department of Biotechnology, Koneru Lakshmaiah Education Foundation (Deemed to Be University), Green Fields, Vaddeswram, AP 522502, India

2 Department of Biotechnology, School of Life Sciences, Vels Institute of Science, Technology and Advanced Studies (VISTAS), Chennai, Tamil Nadu 600117, India

3 Department of Food Science and Biotechnology & Carbohydrate Bioproduct Research Center, Sejong University, Gwangjin District, Seoul, South Korea

4 Department of Pharmaceutical Chemistry & Analysis, School of Pharmaceutical Sciences, Vels Institute of Science, Technology & Advanced Studies (VISTAS), Chennai, Tamil Nadu 600117, India

Published online: 08 December 2025

NCDs. Respiratory diseases are increasing due to environmental pollutants and post viral infection effects. Idiopathic Pulmonary Fibrosis (IPF) represents a progressive lung disease characterized by excessive extracellular matrix (ECM) deposition, resulting in fibrosis and decreased lung function (Sankari et al. 2024). The precise cause of IPF is unclear, but several molecular pathways, including the involvement of matrix metalloproteinase-9 (MMP9), are significant in its development, highlighting its role in ECM degradation and remodelling.

Often initiated by damage to lung lining cells from environmental factors such as smoking or pollutants, the body reacts by producing excessive collagen due to the enzyme MMP-9. This enzyme, primarily expressed by alveolar macrophages, neutrophils, and epithelial cells, is elevated in lung fibrosis patients (Bormann et al. 2022). Excessive collagen leads to scar tissue formation, resulting in stiffer, less functional lung tissue. Idiopathic pulmonary fibrosis (IPF) is manifested through progressive dyspnea, a dry cough, and worsening shortness of breath, ultimately leading to respiratory failure as the condition deteriorates. Dysregulated MMP9 activity disrupts the balance between ECM synthesis and degradation, contributing to the aberrant deposition of collagen and fibrotic tissue formation. Alveolar macrophages, neutrophils, and epithelial cells are the primary sources of MMP9 in the lungs, and its overexpression has been linked to increased fibrosis severity. Inhibiting MMP9 activity presents a promising therapeutic strategy by preventing excessive ECM breakdown and subsequent fibrotic remodeling.

The breakdown of lung tissue and subsequent scar tissue formation can be influenced by MMP9, which also aids in collagen production alongside a hydroxamate inhibitor. MMP9's catalytic site interaction with inhibitors provides critical molecular insights (Leong et al. 2021). In idiopathic pulmonary fibrosis (IPF), two proteins, gelatinase-B and 1GKD, play significant roles. Gelatinase-B contributes to extracellular matrix (ECM) breakdown, resulting in lung damage, while 1GKD, located on type I collagen, is vital for collagen fibril assembly (Mubieya et al. 2024). Structural or functional abnormalities in the 1G-K domain can lead to various connective tissue diseases, emphasizing the need for research into remedies targeting active sites related to MMP9 gene mutations (Rowsell et al. 2002).

In the present study, the 1GKD protein site was chosen for further research on the IPF due to its lesser bond length compared to Gelatinase-B. In-depth studies on 1GKD have provided the active sites and functional domains that can regulate and control the degradation activity of the MMP9 in lung tissue. Using this structural understanding, scientists are creating molecules that can attach to 1GKD specifically and prevent its function (Wu et al. 2024). The creation of these ligands is encouraging as it promises a precise and focused treatment strategy for IPF. The urgency to identify and optimize ligands that are present in active sites capable of inhibiting MMP9 is underscored by the global need for therapeutics. Successful drug development targeting MMP9 could revolutionize the treatment landscape for IPF and lung-related diseases. Some silico methods like ADMET, TOPKAT, and Molecular docking are used for the analysis of MMP9 against IPF (Reddy et al. 2021).

GC–MS analysis was used to identify compounds within the *Mentha piperita L.*(a plant of Mint species) found in tropical regions of South India. This plant belongs to the Lamiaceae family and was taken from the Siddha Ayurveda Institute, Chennai. Recently, *Mentha piperita L.*, a versatile plant with a well-established history in traditional medicine, is increasingly being investigated for its potential therapeutic applications in idiopathic pulmonary fibrosis (IPF) (Ogaly et al. 2018). Studies have demonstrated the anti-inflammatory and anti-cancer properties of terpenes, which are bioactive chemicals derived from *Mentha piperita* L. Some other bioactive substances including flavonoids, rosmarinic acid, and menthol, *Mentha piperita* L. has strong anti-malarial, antimicrobial, anti-bacterial, anti-septic, anti-fibrotic, and antioxidant effects (Espindola et al. 2021a). Due to the above mentioned qualities, it is a potential option for slowing the progression of IPF. Because they contain the majority of the bioactive chemicals, plant leaves were selected.

Carvone derivatives, including D-carvone and L-carvone, have demonstrated various biological activities such as anti-inflammatory and anticancer effects (Morcia et al. 2016). These compounds may influence key signaling pathways involved in inflammation and fibrosis, particularly the transforming growth factor-beta (TGF-β) and mitogen-activated protein kinase (MAPK) pathways. By modulating MMP9 and its associated regulatory mechanisms, carvone derivatives hold the potential for mitigating fibrotic progression, making them promising candidates for further investigation in idiopathic pulmonary fibrosis (IPF) treatment (Espindola et al. 2021a).

While research on the role of *Mentha piperita* L. in IPF remains in its early stages, preliminary findings suggest it may offer a natural and complementary approach to managing the disease. However, rigorous experimental validation, including in vitro and in vivo studies, is essential to establish its therapeutic potential. To address this research gap, we employed computer-aided drug discovery methods. Through molecular docking studies targeting MMP9, we identified promising bioactive compounds, laying the groundwork for future studies in drug development against IPF.

Materials and methods

Sample collection and preparation of solvent extract

The fresh *Mentha piperita* L. (peppermint" which is a cross between watermint and spearmint plants) leaves were collected from the surrounding farmlands of KL University, Vaddeswaram, Guntur, Andhra Pradesh. These leaves were collected from the stem using a floral stem cutter were washed with distilled water thoroughly and dried at room temperature. *Mentha piperita* L. leaves were powdered after three days of surface drying method (drying the leaves in open air) using mortar and pestle and 30 g of powder was used for extraction with methanol using Soxhlet apparatus (Pratyusha et al. 2024).

Soxhlet apparatus

300 ml of methanol was used to extract phytochemical compounds from mint leaves. Before the process, the soxhlet extraction process was performed in glass ware materials and.

the mint leaf powder was packed in No.4 Whatman filter paper to eliminate impurities and particulate matter, which was drenched with 50 ml of methanol. The round bottom flask was filled with 250 ml of methanol in the Soxhlet apparatus. The thimble was placed in the Soxhlet extractor, and the process was initiated from 70 °C until the first cycle was completed. After the first cycle, the temperature was regulated to 55 °C, and the process was carried out for 30 h. The solvent extract was attained after 30 h and underwent drying. Around 210 ml of solvent extract was dried for nine days under a laminar airflow bench. The 4 ml of pure solvent extract of mint leaves was collected in a 15 ml falcon tube (Tarson) and was further subjected to GC–MS analysis (Ramalingam and Rajaram 2018).

Table 1 GC–MS graph of mint leaves extract individual compounds

Compound code	Name of the compound	Retention time	Peak area (%)
MSMP1	Cyclopropane carboxylic acid, 2-methoxy-, methyl ester, trans-	8.111	2.48
MSMP2	(-)-Carvone	13.89	4.5
MSMP3	cis-Dihydrocarvone	14.052	1.39
MSMP4	(-)-. Beta. -Bourbonene	16.825	5.54
MSMP5	Caryophyllene	17.329	4.21
MSMP6	(S,1Z,6Z)-8-Isopropyl-1-methyl-5-methylenecyclodeca-1,6-diene	17.646	1.05
MSMP7	Humulene	17.811	0.54
MSMP8	Naphthalene, 1,2,3,5,6,8a-hexahydro-4,7-dimethyl-1-(1-methylethyl)-,(1S-cis)	18.578	0.66
MSMP9	Trans-Calamenene	18.639	0.73

GC–MS analysis

The methanolic extract of *Mentha piperita* L. leaves was analyzed using gas chromatography–mass spectrometry under standard conditions. Helium was used as the carrier gas at a flow rate of 1 mL/min, and the injector temperature was set at 250 °C. The oven temperature was initially held at 60 °C for 2 min, then programmed to increase at 10 °C/min up to 280 °C, where it was maintained for 10 min. One microliter of the extract was injected in split mode (split ratio 10:1). Compounds were identified by comparing their mass spectra with entries in the NIST library and by cross-referencing with the PubChem database. A total of nine phytochemicals were identified, with (-)-Carvone, cis-Dihydrocarvone, and (-)-ß-Bourbonene being the major constituents (Thamer and Thamer 2023) (Table 1).

Bioactive compound filtration

The drug-likeness characteristics of the GC–MS identified compounds were evaluated based on Lipinski's Rule (Ro5) using the licensed software, Discovery Studio. Prior to analysis, each compound's structure, derived from the GC–MS data, was used to retrieve its SMILES notation via ChemSketch (ACD/ChemSketch Freeware, version 2022.2.3) (Reddy et al. 2022). This methodical approach helps identify compounds with favorable drug-like properties, thereby expediting the selection process for additional pharmacological investigation.

ADMET

ADMET property prediction and physicochemical descriptor computation were done by Dassault Systèmes Biovia Corp.'s Discovery Studio software (v21.1.0.20298). The analysis of ADMET properties involved a careful evaluation of critical parameters, including solubility, Blood–Brain Barrier (BBB) permeability, Plasma Protein Binding (PPB), and AlogP98. Important information about the possible safety, pharmacological profiles, and efficacy of the compounds under investigation was provided by the thorough assessment of these parameters (Roney et al. 2021).

TOPKAT toxicity

In this work, we used the TOPKAT toxicity prediction module available in Discovery Studio, an integrated, offline software platform developed by BIOVIA for simulating and analyzing molecular structures, drug-likeness, ADMET, and toxicity prediction in computational drug discovery, to assess the safety profiles of (-)-carvone and cis-dihydrocarvone, two bioactive molecules derived from *Mentha*

piperita L.. The compounds were prepared in SDF format and uploaded into the software for analysis. Toxicity endpoints were predicted using the FDA Carcinogenicity and Mutagenicity models integrated within TOPKAT. These models apply quantitative structure–toxicity relationship (QSTR) principles, evaluating molecular substructures and electronic features to estimate the likelihood of carcinogenic or mutagenic effects. The outcomes of this computational screening allowed us to prioritize the compounds and gain preliminary safety insights, which guided their further investigation through molecular docking and molecular dynamics simulations.

Protein analysis

The structural information of Protein Data Bank (PDB) entries is extensively summarized online with the PDBsum web server: https://www.ebi.ac.uk/thorntonsrv/databases/pdbsum/ and users can receive full information about Rama chandran plot statistics, protein topology diagrams, ligand interactions, and domain organization from entering a PDB ID: 1GKD or uploading a structure file. The server is also used for the graphical visualization of secondary structures, protein–ligand, and protein–protein interactions along with some other functional information. It includes evolutionary data, active sites of enzymes, and the consequences of mutations. PDBsum is an informative service for structural biologists and bioinformaticians investigating three-dimensional structures of biomolecules, their relations, and functional font size (Manoharan et al. 2025).

Preparation of ligands

Molecular docking simulations, which anticipate the ideal orientation of a ligand molecule upon binding to a target receptor and producing a stable complex, are carried out using Molegro Virtual Docker (2014.6.0.1), a software platform. A crucial step in molecular docking simulations is ligand preparation, which guarantees the proper arrangement and refinement of ligand molecules for ensuing docking investigations. The energy was kept to a minimum until 1500. Molegro Virtual Docker usually offers an easy-to-use interface in addition to features that make ligand preparation procedures go more smoothly. Minimization of energy Users may efficiently prepare ligands for docking simulations by utilizing the software's built-in features and procedures (Gnanaraj et al. 2022).

Selection of targets

Matrix Metalloproteinase 9 (MMP9) is recognized as a key therapeutic target for the drug design against idiopathic pulmonary fibrosis (IPF). The PDB (PDB Id: 1GKD) provided the 3D crystal structures of the MMP9 target. The Molegro Virtual Docker's built-in function was used to regulate protonation. Amino acid sequences with flawed structures were changed appropriately.

Docking studies

The docking approach uses a reference ligand to anticipate the configuration and placement of the ligand within a given binding site. Several phases are often involved in docking, each of which adds to the analysis's complexity. Small compounds are first positioned inside a biological component's active site using docking techniques. These algorithms are used to forecast biological activity and are supplemented by scoring functions that assess molecular interactions and possible targets.

For the docking studies, matrix metalloproteinase-9 (MMP9) was selected as the target protein, and its three-dimensional structural coordinates were retrieved from the Protein Data Bank (PDB ID: 1GKD). Once the disease-associated target was identified, the corresponding structure was downloaded to serve as the basis for further computational analysis. Importantly, the PDB file format frequently has erroneous or non-existent explicit hydrogen assignments and lacks bond order information. Potential binding sites for targets were identified using the Integrated Cavity Detection by MVD technique. After that, the docking radius was adjusted to 15, which covered more than 90% of the protein cavities found. Energy reduction, cavity pose limitations, and H-bond optimization were all enabled when the MolDock SE searching method was chosen. The Tries values were set to 10 min for the minimum, 10 min for the fast, and 30 min for the maximum trials, while the maximums for the iterations, population size, and energy threshold were set at 1500, 50, and 100.00, respectively. Max phase and neighbour distance factor were kept at their default settings of 300 and 1.00, respectively. The energy threshold was likewise turned on in the pose clustering dialog box. A smaller 9.0 Å radius surrounding the active site crevice was covered by the area examined in the docking investigations. A score of 0.50 was given to the water molecules that were replaced during the procedure to account for their existence. The docking scores of active components were compared with *2-amino-n,3,3-trimethyl butanamide* from the Drug Bank in SDF format after ligands were imported into the workspace and ready for docking investigations. For docking investigations utilizing Molegro Virtual Docker offline software, the target was saved in PDB format, and the ligand structures were saved in SDF format (Mukkavilli et al. 2024). The publication by Amador-Falcón et al., (Amador-Falcón

et al. 2013) mentions the inclusions and docked complex of MMP9 and reference ligand (BUM_1449 [A]).

Molecular dynamics

A molecular dynamics simulation of protein–ligand interaction stability and variability helped in understanding the binding mechanism of prospective drug candidates with their targets. Simulations were performed on a Linux system using the Desmond module from the Maestro simulation package (Schrödinger, Inc.) (Khan and Roy, 2022). To take into account complex protein–ligand interactions, the TIP3 water model was used, with boundaries set within a box. Na+and Cl−salts were included in concentrations of 0.15 M to balance the system; all simulations were performed in the NPT ensemble, maintaining p = 1.01325 bar and T = 300 K; energy evaluations used the OPLS-4 force field, and data were collected every 50 ps. The run for complexes of MSMP4 with protein 1GKD was over 100 ns long. MD simulation data were thoroughly analyzed in Schrödinger using the Desmond module. Techniques such as the simulation interaction diagram were also used as an added analysis in the study. Metrics such as root mean square deviation (RMSD), root mean square fluctuation (RMSF), and protein–ligand interaction analysis in the simulated trajectories were used to evaluate the stability of the ligand–protein complexes of the selected hits (Manoharan et al. 2025).

Results and discussion

GC–MS analysis

The chromatogram shows the relationship between retention time (x-axis) and intensity (y-axis) (Fig. 1), which indicates how long each compound takes to pass through the column and its relative abundance. The most prominent peak was recorded at 14.824 min with an intensity of about 30,177,690, identifying it as the major constituent of the extract. Additional smaller peaks at 8.111, 13.890, 14.052, 16.825, 17.329, 17.646, and 17.811 min correspond to compounds present in lower concentrations. This analysis provided a clear chemical profile of the extract and highlighted the principal active constituents (Table 2).

Bioactive compound filtration analysis

All phytoconstituents from Mentha piperita, including MSMP2 and MSMP3, complied with Veber's rule and Lipinski's drug-likeness criteria (Table 3). However, most compounds, except MSMP2 and MSMP3, did not meet the blood–brain barrier and plasma protein binding requirements. These two compounds also showed favourable solubility values, justifying their selection for further analysis.

ADMET profiling illustrated the relationship between polar surface area (ADMET_PSA_2D) and lipophilicity (ADMET_AlogP98) (Fig. 2). The inverse trend between polarity and hydrophobicity indicated that highly polar compounds had reduced membrane permeability. Outliers identified in the plot may represent candidates with unique pharmacokinetic features requiring further study.

Toxicity prediction using the Weight of Evidence (WOE) and TOPKAT modules classified (-)-carvone and

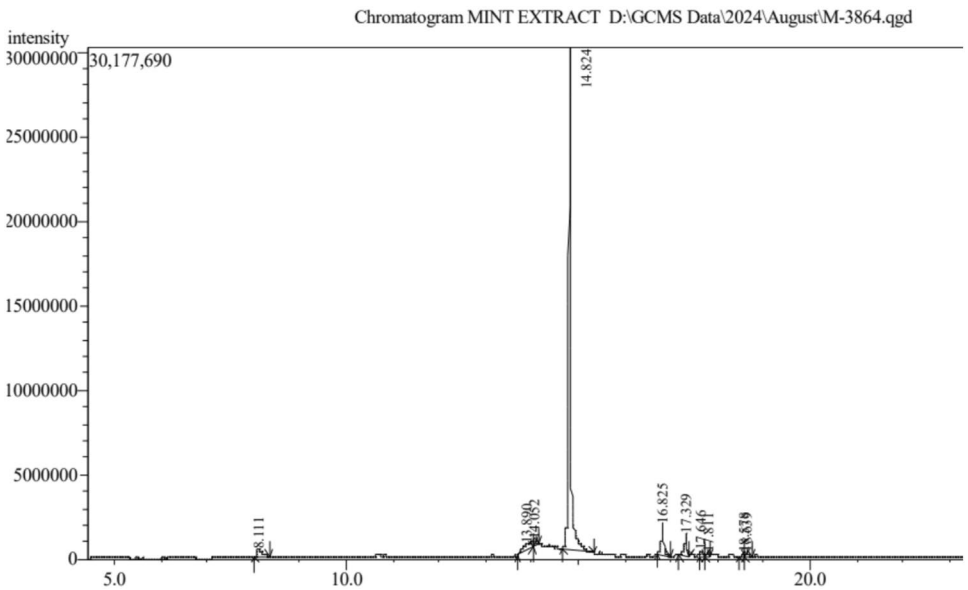

Fig. 1 Gas chromatography-mass spectrometry (GC–MS) chromatogram of methanolic extract from *Mentha piperita* L. leaves. The x-axis represents retention time (minutes) and the y-axis shows peak intensity (abundance). The major peak at 14.824 min (intensity ~ 30,177,690) corresponds to (-)-carvone, the principal constituent. Additional peaks represent: cyclopropane carboxylic acid derivative (8.111 min), cis-dihydrocarvone (14.052 min), (-)-β-bourbonene (16.825 min), caryophyllene (17.329 min), germacrene (17.646 min), humulene (17.811 min), δ-amorphene (18.578 min), and trans-calamenene (18.639 min). Peak areas correlate with relative compound abundance in the extract

Table 2 Compounds of mint leaves extract of *Mentha spicata* (spearmint) and *Mentha piperita* (peppermint)

Compound Code	Name of the Compound	Functions	Structures	Smile notation	Chemical Formula	Molecular Weight	Ref
MSMP1	Cyclopropane carboxylic acid, 2-methoxy-, methyl ester, trans-	Plant defense, Signalling, and interaction with other microorganisms	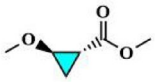	O=C(OC)C1CC1OC	C6 H10 O3	130.143	20,21
MSMP2	(-)-Carvone	Anti-septic, Mosquito repellent, flavoring agent, and essential oil.	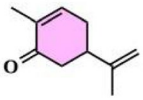	CC1=CCC(CC1=O)C(C)=C	C10 H14 O	150.221	22,23
MSMP3	cis-Dihydrocarvone	Plant defense, attractants, interaction with others, and microorganism's essential oil.	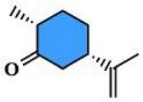	CC1CCC(CC1=O)C(C)=C	C10 H16 O	152.237	24,25
MSMP4	(-)-.beta.-Bourbonene	antimicrobial, anti-inflammatory, and potential antitumor effects.		CC12CCC(C(C)C)C1C1C2CCC1=C	C15 H24	204.357	26,27
MSMP5	Caryophyllene	antibacterial, antioxidant, gastroprotective, anxiolytic, anti-inflammatory, and herbal medicine.	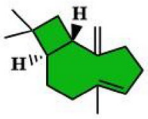	CC1(C)CC2C1CC\C(C)=C/CCC2=C	C15 H24	204.357	28,29
MSMP6	(S,1Z,6Z)-8-Isopropyl-1-methyl-5-methylenecyclodeca-1,6-diene (Germacrene)	aromatherapy, and potential therapeutic applications	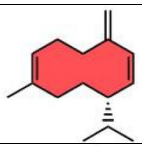	C/C=1CCC(\C=C/C(=C)CC\C=1)C(C)C	C15 H24	204.357	30,31
MSMP7	Humulene	Suppress appetite, anti-inflammatory and aromatic applications	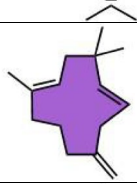	CC/1(C)C\C=C(/C)CC\C=C(/C)C\C=C\1	C15 H24	204.357	32,33
MSMP8	Naphthalene, 1,2,3,5,6,8a-hexahydro-4,7-dimethyl-1-(1-methylethyl)-,(1S-cis) ((+)-δ-Amorphene)	Antinociceptive(Inhibition of Prostaglandins), antimalarial and anti-cancer	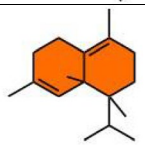	CC=1CCC(C2C=C(C)CCC2=1)C(C)C	C15 H24	204.357	34,35
MSMP9	Trans-Calamenene	Useful in Neurogenesis, reduction of oxidative stress, and aromatic applications	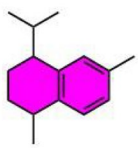	CC1CCC(c2cc(C)ccc21)C(C)C	C15 H22	202.341	36,37

cis-dihydrocarvone as non-carcinogenic and non-toxic, with negligible skin sensitization, whereas most other compounds showed carcinogenic or irritant potential (Table 4**,** Fig. 3). These results support (-)-carvone and cis-dihydrocarvone as safe and promising candidates for further molecular docking and dynamics studies targeting MMP9.

Table 3 Predicted values for solubility, blood–brain barrier, plasma protein binding, AlogP98

Compound name	ADME	*Solubility	**BBB (Blood–brain barrier prediction)	EXT_PPB (Plasma protein binding)	***AlogP98
MSMP4	Fail	−5.364	1.151	1.353	4.222
MSMP5	Fail	−5.688	1.315	2.734	4.753
MSMP6	Fail	−5.643	1.433	3.454	5.135
MSMP9	Fail	–	–	2.877	–
MSMP7	Fail	−5.699	1.402	0.676	5.035
MSMP3	Pass	−3.12	0.357	−2.435	2.54
MSMP8	Fail	−5.713	1.373	1.663	4.939
MSMP2	Pass	−3.089	0.345	−1.524	2.509
MSMP1	Fail	−0.594	−0.684	−1.702	0.585

*Solubility: High: > 1 mg/mL, Moderate:0.1–1 mg/mL, Low: < 0.1 mg/mL

**Permeability coefficient (Papp) value above 10×10^{-6} cm/s is considered indicative of good BBB penetration

***AlogP98 (Octanol–water partition coefficient at pH 7.4: Values typically range from s−2 to 6, with higher values indicating greater hydrophobicity)

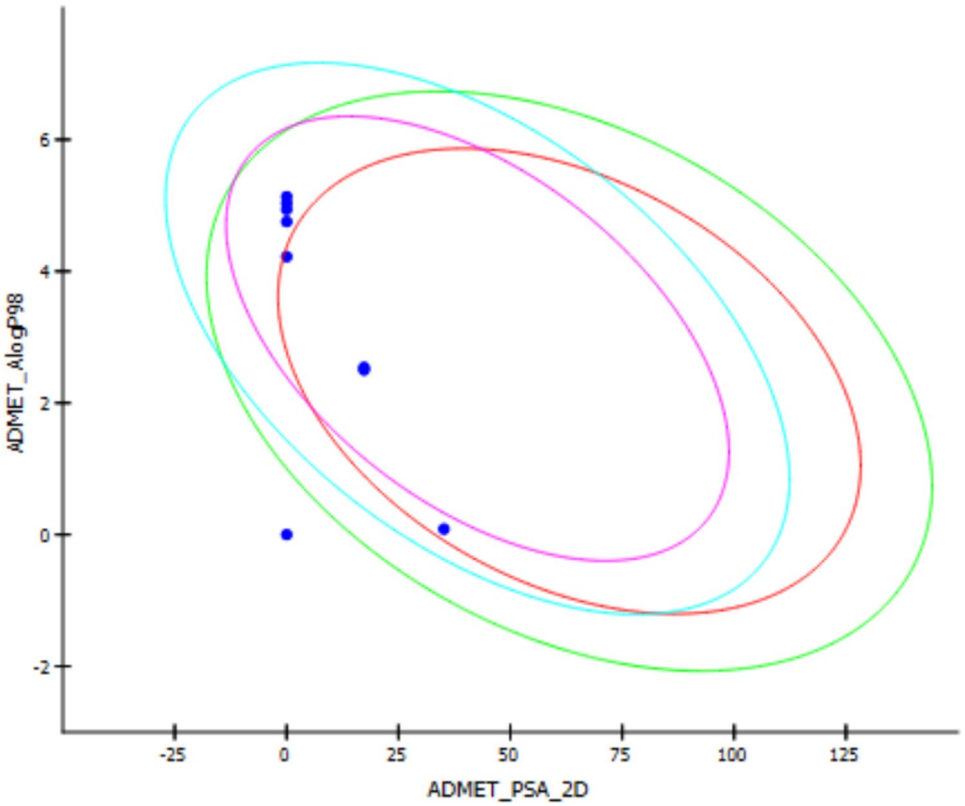

Fig. 2 ADMET scatter plot showing the relationship between polar surface area (ADMET_PSA_2D) and lipophilicity (ADMET_AlogP98) for the nine identified compounds. Blue dots represent individual compounds (MSMP1-MSMP9). Colored ellipses indicate confidence intervals: red circle = 95% absorption confidence, green circle = 99% absorption confidence, pink circle = 95% blood–brain barrier (BBB) penetration, blue circle = 99% BBB penetration. The inverse relationship between PSA (y-axis, indicating polarity) and AlogP98 (x-axis, indicating hydrophobicity) demonstrates that more polar compounds exhibit lower membrane permeability. Compounds falling within the ellipses meet favorable pharmacokinetic criteria for oral bioavailability and BBB penetration

Protein analysis

Ramachandran plot analysis using PROCHECK demonstrated that 88.4% (229 residues) of the model were positioned in the most favoured regions (A, B, L), 10.0% (26 residues) in additional allowed regions, and 1.5% (4 residues) in generously allowed regions, with none occurring in disallowed zones. This distribution indicates excellent stereochemical quality and structural stability of the protein model. Among the 314 non-glycine and non-proline residues analysed, the G-factor value of 0.33 confirmed acceptable bond lengths and angles (> 0.5), suggesting a well-refined geometry without significant deviations (Fig. 4).

Key hydrogen bonds and π–π stacking interactions were observed between His405 (A), Pro421 (A), and Tyr423 (A), with bond lengths of 2.70 Å and 3.12 Å, respectively. The Zn1450 (A) residue exhibited a crucial coordination role, further stabilising the structure, while hydrophobic residues such as Leu188 (A) and Met422 (A) contributed to maintaining tertiary integrity. The close spatial proximity of

Table 4 Predicted values for AMES mutagenicity, WOE (weight of evidence), DTP (developmental toxicity profiling), skin sensitization

Compound name	*AMES mutagenicity	**WOE	***DTP	****Skin sensitization
MSMP4	Non-mutagen	Carcinogen	Toxic	Irritant
MSMP5	Non-mutagen	Carcinogen	Toxic	Irritant
MSMP6	Non-mutagen	Carcinogen	Toxic	Irritant
MSMP9	Non-mutagen	Carcinogen	Non-toxic	Irritant
MSMP7	Non-mutagen	Carcinogen	Toxic	Irritant
MSMP3	Non-mutagen	Non-carcinogen	Non-toxic	Irritant
MSMP8	Non-mutagen	Carcinogen	Non-toxic	Irritant
MSMP2	Non-mutagen	Carcinogen	Non-toxic	Irritant
MSMP1	Non-mutagen	Carcinogen	Toxic	Non-irritant

these interacting residues supports stable binding with the reference ligand BUM_1449 (A).

Cleft analysis revealed two major binding pockets: Cleft 1, the largest by volume (2654.02 $Å^3$, average depth 10.02 Å), associated with residues 2, 7, 8, and 15, represents the principal ligand-binding region; Cleft 2, with an R1 ratio of 0, remains accessible and may function as an auxiliary interaction site. Collectively, these findings confirm that the model exhibits robust stereochemical reliability and a stable protein–ligand complex configuration (Fig. 5).

Molecular docking analysis and binding affinity evaluation of ligands

Each compound's binding affinity to the target receptor was assessed using the MolDock score, where lower (more negative) values indicate stronger interactions. Molecular docking analysis revealed distinct binding affinities among the tested ligands. Among them, (−)-β-bourbonene (MSMP4) exhibited the strongest interaction with the MMP9 receptor, achieving a MolDock score of − 118.385, a rerank score of − 75.7073, and a hydrogen bond energy of 0, reflecting stable and favourable binding (Noumi et al. 2023; Gurung et al. 2021). In contrast, cyclopropane carboxylic acid, 2-methoxy-, methyl ester, trans- (MSMP1) showed a lower affinity (MolDock score − 71.115), while compounds such as trans-calamenene (MSMP9), humulene (MSMP7), and cis-dihydrocarvone (MSMP3) demonstrated moderate to weak binding, consistent with their less negative scores and minimal hydrogen-bonding interactions.

These results highlight clear structure–activity relationships (SAR) that may guide further ligand optimisation. Notably, the strong docking performance of MSMP4 suggests its potential as a promising MMP9 inhibitor for subsequent in vitro and in vivo validation, whereas other compounds may require structural refinement to enhance receptor binding (Table 5).

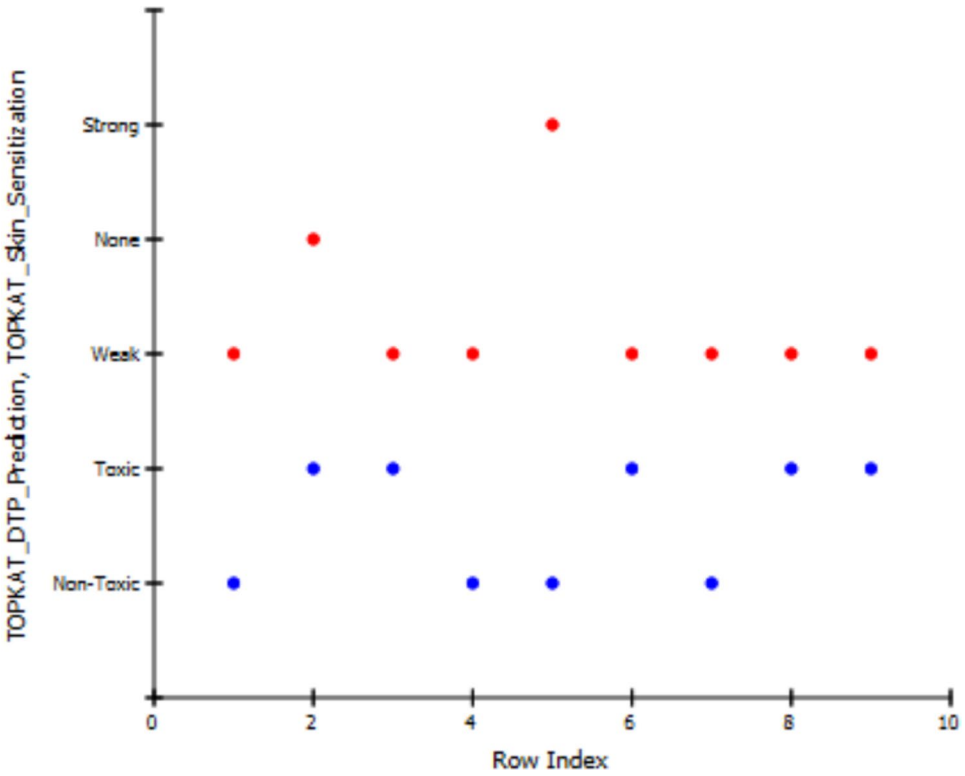

Fig. 3 TOPKAT toxicity predictions for developmental toxicity potential (DTP) and skin sensitization of phytochemicals from *Mentha piperita* L. The vertical axis represents predicted toxicity scores, while the horizontal axis shows compound codes (MSMP1-MSMP9). Red bars indicate compounds predicted to cause skin sensitization or developmental toxicity. Blue bars represent compounds classified as non-toxic with negligible sensitization potential. (-)-Carvone (MSMP2) and cis-dihydrocarvone (MSMP3) show the lowest toxicity profiles, supporting their selection as lead therapeutic candidates. Higher toxicity scores for compounds like MSMP1, MSMP4-MSMP8 suggest the need for careful dosage optimization if pursued further

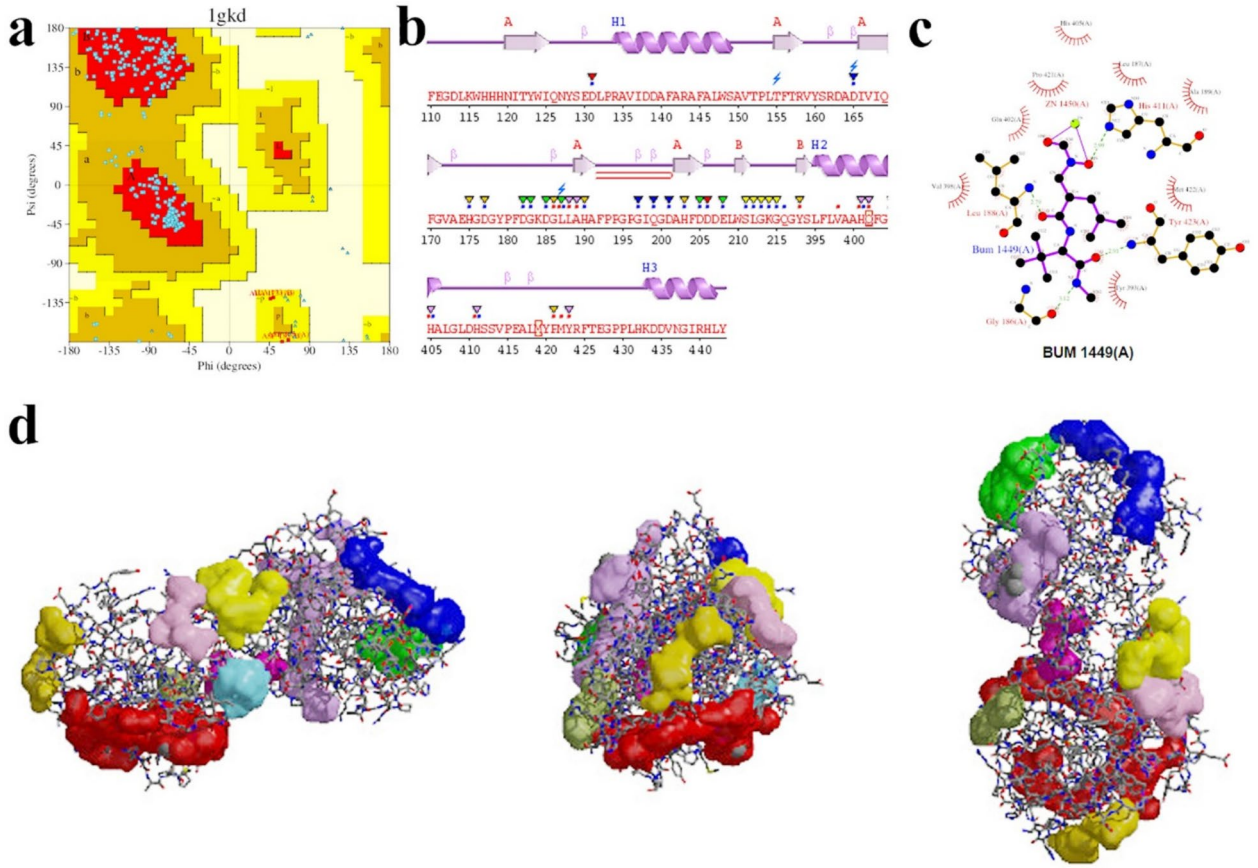

Fig. 4 Structural validation and molecular interactions of MMP9 protein (PDB ID: 1GKD) with reference ligand BUM_1449[A]. **a** Ramachandran plot showing 88.4% of residues in most favored regions (A, B, L), 10.0% in additional allowed regions (a, b, l, p), and 1.5% in generously allowed regions, with no residues in disallowed regions, confirming good stereochemical quality. **b** Secondary structure diagram displaying helical regions (H1, H2, H3) and key structural elements. **c** Two-dimensional molecular network showing hydrogen bonding interactions between BUM_1449[A] and residues His405(A), Pro421(A), and Tyr423(A) (bond lengths: 2.70 Å and 3.12 Å), with Zn1450(A) coordination stabilizing the complex. **d** Three-dimensional protein surface representations highlighting binding pocket topology and active site architecture. Arrows and triangles indicate critical residues involved in structural stability

Post-docking analysis of ligand and protein interaction

Analysis of post-docking ligand and protein interaction was performed by BIOVIA Discovery Studio Visualizer. Subsequently, the protein MMP9, (-)-.beta.-Bourbonene, exhibited a hydrophobic bond and H-bond with interacting molecules including LEU(188), LEU(397), VAL(398), HIS(401), PRO(415), GLU(416), ALA(417), LEU(418), TYR(420), PRO(421), MET(422), TYR(423) and ARG(424) as mentioned in Table 6.

Nine different chemicals were discovered after a thorough examination of the mint plant using GC–MS. One of these molecules demonstrated particularly good docking scores, indicating the possibility of its therapeutic effectiveness.

However, most of the phytochemicals didn't match the ADMET (absorption, distribution, metabolism, excretion, and toxicity) standards, therefore further study is needed to lessen these drawbacks. MMP9 of (-)- beta-Bourbonene had a MolDock score of − 149.574, which was higher than the reference medication 2-Amino-N,3,3-Trimethylbutanamide's value of -125.204. A viable medication option with few adverse effects for the treatment of idiopathic pulmonary fibrosis may be found by examining the impact of allergic reactions (in vitro studies) and it shows adverse effects on pregnancy and breastfeeding women during this cycle. As well as investigating the pharmacokinetic characteristics of phytoconstituents to clarify their absorption, distribution, metabolism, and excretion profile, future research efforts might focus on evaluating the in vitro and in vivo impacts of (-)-beta -Bourbonene on allergic responses.

Molecular dynamics analysis

Root mean square deviation (RMSD) analysis (Fig. 6a) revealed the conformational stability of the protein–ligand complex throughout the 100 ns simulation. The protein

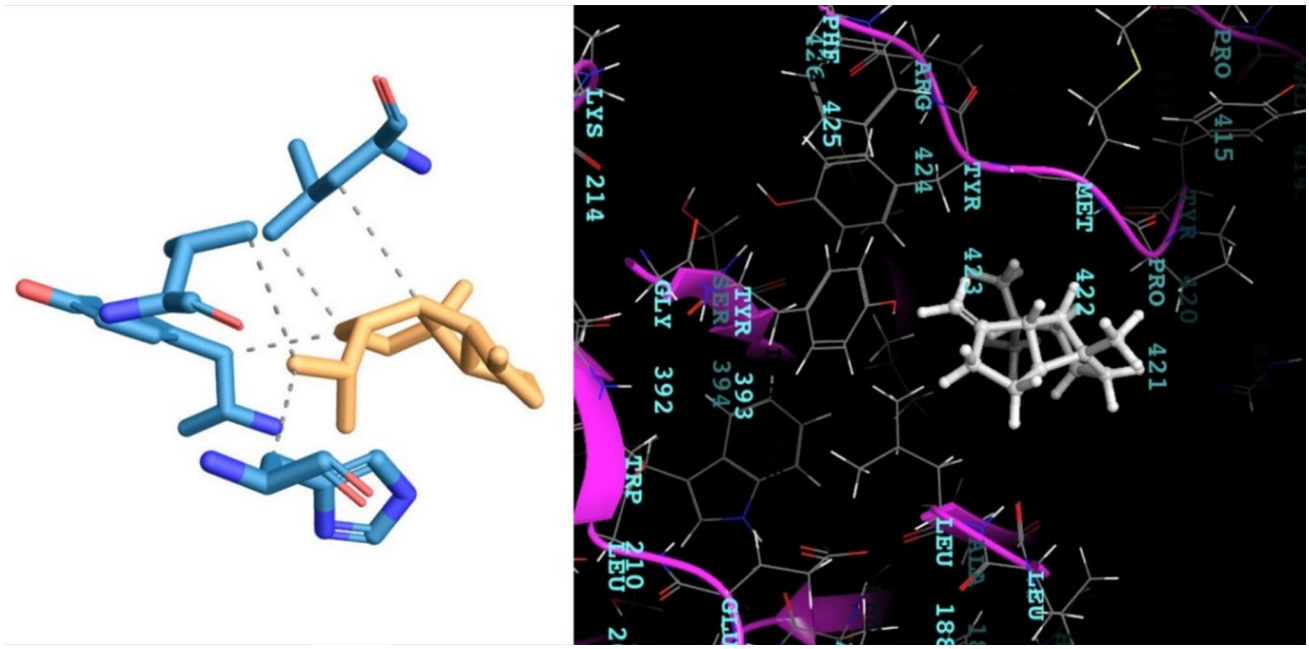

Fig. 5 Molecular docking interactions between (-)-β-bourbonene (MSMP4) and MMP9 protein (1GKD). Left panel: Three-dimensional visualization showing the ligand (cyan sticks) positioned within the MMP9 binding pocket (gray surface), with key amino acid residues displayed. Right panel: Two-dimensional interaction diagram illustrating binding forces: green circles = Van der Waals interactions (LEU188, PRO415, GLU416, ALA417, MET419, TYR420, PRO421, MET422, TYR423, THR426, PRO430); pink circles = alkyl and pi-alkyl interactions (LEU397, VAL398, HIS401, LEU418, ARG424). The MolDock score of -118.385 indicates strong binding affinity. Bond distances and interaction types support stable complex formation

Table 5 The binding affinity of MSMP compounds and 1GKD protein

Name	Ligand	MolDock score	Rerank score	HBond
BUM_1449 [A]	BUM_1449 [A]	−125.204	−102.404	−8.44903
MSMP4	(-)-. beta.-Bourbonene	−118.385	−75.7073	0
MSMP5	Caryophyllene	−100.034	−4.99447	0
MSMP6	(S,1Z,6Z)-8-Isopropyl-1-methyl-5-methylenecyclodeca-1,6-diene (Germacrene)	−98.1502	−16.3578	0
MSMP9	Trans-Calamenene	−96.6122	−15.714	0
MSMP7	Humulene	−95.2081	−60.1886	0
MSMP3	cis-Dihydrocarvone	−87.4661	−76.6508	0
MSMP8	Naphthalene, 1,2,3,5,6,8a-hexahydro-4,7-dimethyl-1-(1-methyl ethyl)-,(1S-cis) ((+)-δ-Amorphene)	−87.4658	−49.2298	0
MSMP2	(-)-Carvone	−84.2184	−73.3933	0
MSMP1	Cyclopropane carboxylic acid, 2-methoxy-, methyl ester, trans-	−71.115	−62.861	−2.48996

Table 6 Ligand-receptor interaction analysis

Target protein	Phyto compound	Binding score	Bond type		
			Pi-alkyl interaction	Alkyl interaction	Van der Waals interaction
1GKD	MSMP4	−118.385	HIS (401)	LEU (397) VAL (398) LEU (418) ARG (424)	LEU (188) PRO (415) GLU (416) ALA (417) MET (419) TYR (420) PRO (421) MET (422) TYR (423) THR (426) PRO (430)

RMSD increased gradually from 1.8 to 7.2 Å, reflecting normal structural flexibility during equilibration, whereas

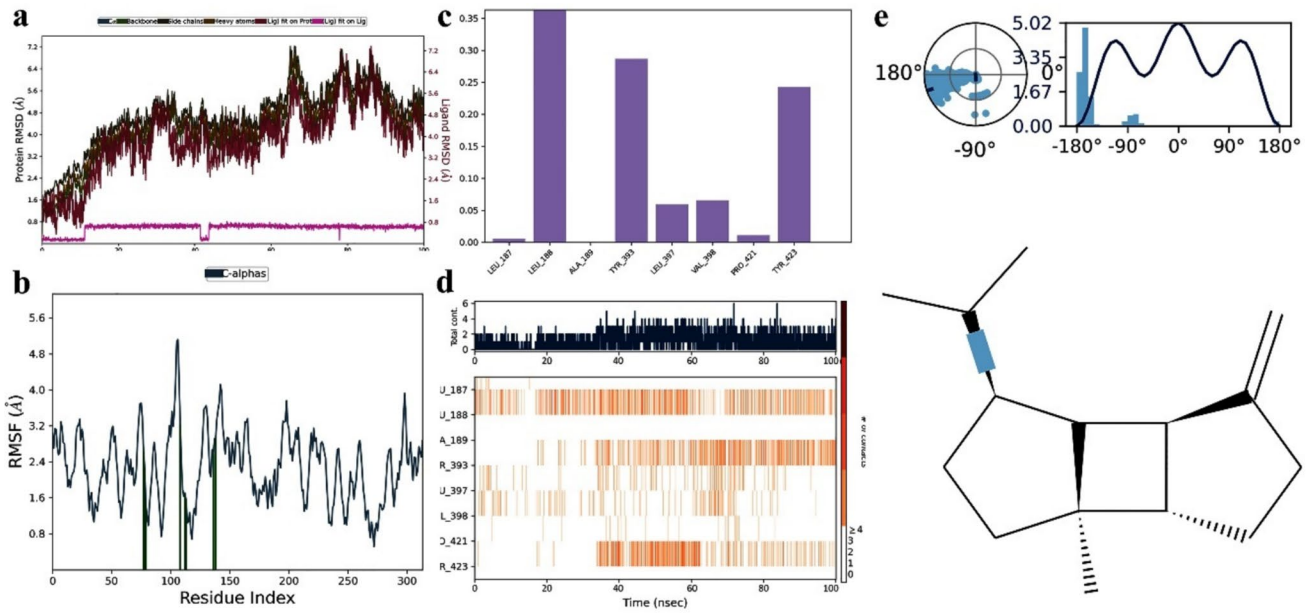

Fig. 6 Molecular dynamics simulation analysis of MMP9-ligand complex over 100 ns. **a** Root mean square deviation (RMSD) of protein backbone (blue), side chains (orange), heavy atoms (gray), and ligand (green) as a function of simulation time. The ligand RMSD stabilizes at ~ 0.8 Å, indicating minimal conformational drift and stable binding. Protein RMSD ranges from 1.8 to 7.2 Å, reflecting normal structural flexibility. **b** Root mean square fluctuation (RMSF) per residue, with prominent peaks between residues 100–130 indicating flexible loop regions potentially involved in ligand accommodation. **c** Contact frequency histogram showing the number of interactions maintained by each residue throughout the simulation. LYS118 and ALA119 exhibit the highest contact frequencies, suggesting critical involvement of these residues in maintaining protein–ligand stability and overall complex integrity during the simulation

the ligand RMSD remained steady at approximately 0.8 Å, indicating minimal displacement and stable binding within the active site. The consistent ligand positioning demonstrates robust intermolecular interactions, confirming that the complex maintained structural integrity under dynamic conditions—an essential characteristic for therapeutic reliability.

Root mean square fluctuation (RMSF) analysis (Fig. 6b) identified local flexibility among amino-acid residues, with prominent peaks observed between residues 100 and 130. These fluctuations correspond to loop or surface regions that may facilitate conformational adaptability during ligand accommodation and binding. The overall RMSF pattern supports the dynamic yet stable nature of the protein backbone during the simulation.

Protein–ligand interaction profiles were further evaluated through contact frequency and timeline analyses (Fig. 6c–d). Residues such as LYS118 and ALA119 exhibited notably high contact frequencies, highlighting their critical role in maintaining complex stability. The contact timeline illustrated periodic formation and dissociation of non-covalent interactions, suggesting dynamic reorientation of the ligand while preserving overall binding equilibrium.

Ligand torsional angle analysis (Fig. 6e) showed minimal angular variation throughout the simulation, confirming that the compound retained a consistent conformation despite protein flexibility. This observation aligns with the stable ligand RMSD and indicates that the binding pose achieved equilibrium early in the simulation.

Collectively, RMSD, RMSF, and interaction analyses confirm that the MMP9–ligand complex remained dynamically stable, with limited conformational drift, strong intermolecular contacts, and adaptive flexibility in specific regions that support sustained and effective binding.

Conclusion

Non-communicable diseases (NCDs) such as diabetes, cancer, cardiovascular disorders, and chronic respiratory illnesses remain a serious global health burden, often arising from lifestyle choices and environmental factors. Among them, idiopathic pulmonary fibrosis (IPF) stands out as a progressive and life-threatening lung condition of unknown origin. IPF is marked by excessive collagen buildup, which causes the lungs to stiffen, reduces elasticity, and ultimately leads to respiratory failure. In this work, mint extract was evaluated for its therapeutic potential because of its established anti-inflammatory and anticancer properties. Gas chromatography–mass spectrometry (GC–MS) revealed nine active compounds, which were subsequently analyzed through computational methods. Of these, (-)-carvone and

cis-dihydrocarvone satisfied drug-likeness requirements and displayed favorable interactions with MMP9, a protein involved in IPF. Although (-)-β-bourbonene showed stronger binding, it did not pass toxicity assessment. Molecular dynamics simulations further confirmed the stability and binding efficiency of (-)-carvone and cis-dihydrocarvone, highlighting them as promising candidates for IPF therapy. However, experimental validation is essential to establish their safety and effectiveness.

Funding No funding was received for this research.

Declarations

Conflict of interest There are no relevant financial or non-financial competing interests to report.

References

Amador-Falcón L, Rodríguez-Clavijo D, Baldiris-Ávila R, Valdiris-Ávila V, Salgado-Morán G, Glossman-Mitnik D, Vivas-Reyes R (2013) Virtual screening: using molecular docking and 3D-QSAR analysis of matrix metalloproteinase inhibitors. J Chin Chem Soc 60(10):1212–1224

Bormann T, Maus R, Stolper J, Tort Tarrés M, Brandenberger C, Wedekind D, Maus UA (2022) Role of matrix metalloprotease-2 and MMP-9 in experimental lung fibrosis in mice. Respir Res 23(1):180

Espindola MS, Habiel DM, Coelho AL, Stripp B, Parks WC, Oldham J, Hogaboam CM (2021a) Differential responses to targeting matrix metalloproteinase 9 in idiopathic pulmonary fibrosis. Am J Respir Crit Care Med 203(4):458–470

Gnanaraj C, Sekar M, Fuloria S, Swain SS, Gan SH, Chidambaram K, Fuloria NK (2022) In silico molecular docking analysis of karanjin against alzheimer's and parkinson's diseases as a potential natural lead molecule for new drug design, development and therapy. Molecules 27(9):2834

Gurung AB, Ali MA, Lee J, Farah MA, Al-Anazi KM (2021) Molecular docking and dynamics simulation study of bioactive compounds from *Ficus carica* L. with important anticancer drug targets. PLoS ONE 16(7):e0254035

Khan K, Roy K (2022) In silico modeling of environmental toxicity of drugs. Contemporary chemical approaches for green and sustainable drugs. Elsevier, Amsterdam, pp 129–154

Kitole FA, Lihawa RM, Mkuna E (2024) Comparative analysis on communicable and non-communicable diseases on catastrophic spending and impoverishment in Tanzania. Glob Soc Welf 11(2):123–134

Leong E, Bezuhly M, Marshall JS (2021) Distinct metalloproteinase expression and functions in systemic sclerosis and fibrosis: what we know and the potential for intervention. Front Physiol 12:727451

Liu H, Yin P, Qi J, Zhou M (2024) Burden of non-communicable diseases in China and its provinces, 1990–2021: results from the Global Burden of Disease Study 2021. Chin Med J 137(19):2325–2333

Manoharan A, Theivendren P, Sharma M, Kunjiappan S, Govindaraj S, Pavadai P (2025) Design, molecular modelling, synthesis, characterization studies of novel N-(7-(substituted benzylidene)-4-phenyl-4, 5, 6, 7-tetrahydro-3H-cyclopenta [d] pyrimidin-2-yl)-1-(substituted phenyl) methanimine against breast cancer. J Iran Chem Soc. https://doi.org/10.1007/s13738-024-03169-6

Morcia C, Tumino G, Ghizzoni R, Terzi V (2016) Carvone (*Mentha spicata* L.) oils. Essential oils in food preservation, flavor and safety. Academic Press, Washington, pp 309–316

Mubieya O, Todd JL, Neely ML, Kaner RJ, Lasky JA, Namen A et al (2024) Associations of circulating matrix metalloproteinases and tissue inhibitors of matrix metalloproteinases with clinically relevant outcomes in idiopathic pulmonary fibrosis: data from the IPF-PRO Registry. PLoS ONE 19(10):e0312044. https://doi.org/10.1371/journal.pone.0312044

Mukkavilli V, Ramakrishnan G, Gujjula KR, Chamarthy S, Mekala JR (2024) Molecular understanding and pharmacological potency of plant-derived compounds in colorectal cancer (CRC): a critical analysis and future perspectives. Cell Biochem Biophys. https://doi.org/10.1007/s12013-024-01370-1

Noumi E, Ahmad I, Adnan M, Merghni A, Patel H, Haddaji N, De Feo V (2023) GC/MS profiling, antibacterial, anti-quorum sensing, and antibiofilm properties of *Anethum graveolens* L. essential oil: molecular docking study and in-silico ADME profiling. Plants 12(10):1997

Ogaly HA, Eltablawy NA, Abd-Elsalam RM (2018) Antifibrogenic influence of *Mentha piperita* L. essential oil against CCl4-induced liver fibrosis in rats. Oxid Med Cell Longev 2018(1):4039753

Pratyusha BB, Samuvel RMS, Nivetha S, Bhuvaneshwari V, Muralidharan K, Swain D, Ramalingam V (2024) LC-HRMS analysis of corn mint *Mentha arvensis* L. for anticancer activity against triple-negative breast cancer targeting inflammatory and apoptosis signaling pathways. New J Chem 48(2):760–769

Ramalingam V, Rajaram R (2018) Enhanced antimicrobial, antioxidant and anticancer activity of *Rhizophora apiculata*: an experimental report. 3 Biotech 8:1–13

Reddy GK, Reddy VN, Phavethra S, Bhavani A, Vineeth AJ, Reddy AVV (2021) In-silico ADME and docking-based virtual screening study aiming at the Sigma-covalent inhibition of SARS-CoV-2 RdRp. J Pharma Res Int 33(54B):321–336

Reddy K, Reddy N, Nadeem Siddiqui SRG, Renukuntla A, Panjala N (2022) Molecular docking and bioactivity studies of covalent inhibitors targeting rdrp of sars-cov-2. Rasayan J Chem 15(4):2666–2675

Roney M, Huq AM, Rullah K, Hamid HA, Imran S, Islam MA, Mohd Aluwi MFF (2021) Virtual screening-based identification of potent DENV-3 RdRp protease inhibitors via in-house usnic acid derivative database. J Comput Biophys Chem 20(08):797–814

Rowsell S, Hawtin P, Minshull CA, Jepson H, Brockbank SM, Barratt DG, Pauptit RA (2002) Crystal structure of human MMP9 in complex with a reverse hydroxamate inhibitor. J Mol Biol 319(1):173–181

Sankari A, Chapman K, Ullah S (2024) Idiopathic Pulmonary Fibrosis. StatPearls. StatPearls Publishing, Treasure Island

Siiba A, Kangmennaang J, Baatiema L, Luginaah I (2024) The relationship between climate change, globalization and non-communicable diseases in Africa: a systematic review. PLoS ONE 19(2):e0297393

Thamer FH, Thamer N (2023) Gas chromatography–mass spectrometry (GC-MS) profiling reveals newly described bioactive compounds in *Citrullus colocynthis* (L.) seeds oil extracts. Heliyon. https://doi.org/10.1016/j.heliyon.2023.e16861

Wu Z, Shi R, Yan S, Zhang S, Lu B, Huang Z, Ji L (2024) Integrating network pharmacology, experimental validation, and molecular docking to reveal the alleviation of Yinhuang granule on idiopathic pulmonary fibrosis. Phytomedicine 128:155368